β-Sheet Proteins with Nearly Identical Structures Have Different Folding Intermediates[†]

Paula M. Dalessio and Ira J. Ropson*

Department of Biochemistry and Molecular Biology, The Pennsylvania State University College of Medicine, Hershey, Pennsylvania 17033

Received August 19, 1999; Revised Manuscript Received December 3, 1999

ABSTRACT: The folding mechanisms of two proteins in the family of intracellular lipid binding proteins, ileal lipid binding protein (ILBP) and intestinal fatty acid binding protein (IFABP), were examined. The structures of these all-β-proteins are very similar, with 123 of the 127 amino acids of ILBP having backbone and C_β conformations nearly identical to those of 123 of the 131 residues of IFABP. Despite this structural similarity, the sequences of these proteins have diverged, with 23% sequence identity and an additional 16% sequence similarity. The folding process was completely reversible, and no significant concentrations of intermediates were observed by circular dichroism or fluorescence at equilibrium for either protein. ILBP was less stable than IFABP with a midpoint of 2.9 M urea compared to 4.0 M urea for IFABP. Stopped-flow kinetic studies showed that both the folding and unfolding of these proteins were not monophasic, suggesting that either multiple paths or intermediate states were present during these processes. Proline isomerization is unlikely to be the cause of the multiphasic kinetics. ILBP had an intermediate state with molten globule-like spectral properties, whereas IFABP had an intermediate state with little if any secondary structure during folding and unfolding. Double-jump experiments showed that these intermediates appear to be on the folding path for each protein. The folding mechanisms of these proteins were markedly different, suggesting that the different sequences of these two proteins dictate different paths through the folding landscape to the same final structure.

Protein folding continues to be one of the major unresolved issues in biochemistry. It is not clear how the sequence of a protein encodes the final structure and the mechanism by which that structure is achieved. Most proteins have been shown to approximate a two-state folding mechanism at equilibrium with significant concentrations of only the completely native and unfolded states present. However, kinetic studies have shown that many of these same proteins fold via states with spectral properties unlike those of either the native or the unfolded form. Classically, these kinetic states were thought to be caused by the presence of defined structural intermediates on the folding pathway, which were considered necessary for proteins to avoid time-consuming searches through all the available conformations (*1*).

Recently, a new conceptual model for folding involving energy "funnels" has been described, and is based on theoretical studies of simplified models for the energetics of protein folding (reviewed in ref *2*). In these models, many potential routes to the native state over a complex energy landscape are possible. Some protein molecules may proceed directly to the native state without encountering any significant energy barriers or local energetic minima. Other molecules are trapped in a variety of metastable conformations that must be partially or completely rearranged before the native structure can be obtained. The multiphasic kinetics observed during the folding process are caused by these "trapped" conformation states. This view of the protein folding process does not exclude the classical model, since there could be proteins that fold via defined structural intermediates. This model emphasizes the enormous variety of conformations in the unfolded state, and the likelihood that this initial structural heterogeneity results in multiple routes to the native state.

One means of experimentally examining these models for protein folding is to compare the folding mechanisms of structurally similar proteins. These studies address a very simple question: Do proteins with different sequences achieve the same final structure in the same fashion? According to the classical model for folding, the mechanism of folding should be evolutionarily conserved, since the sequence encodes the final structure and the structures of the intermediates on the folding pathway (*3*−*6*). The funnel model predicts that related proteins could follow very different paths to the same end state, and thus have different observed folding mechanisms. These paths would be caused by alternative sequences having different structures in the unfolded state and/or different locally stabilized structures acting as folding initiation sites.

The few previous studies of the folding of structurally homologous proteins have led to the generalization that proteins with similar structures have similar folding mechanisms (*5*, *7*−*11*). However, these comparisons were made for protein families that had a high degree of sequence identity, had disulfide bonds, or were largely α-helical. These

[†] Support for this project was provided by a grant to I.J.R. from NSF (MCB94-05282).

* To whom correspondence should be addressed. Phone: (717) 531-4064. Fax: (717) 531-7072. E-mail: iropson@psu.edu.

10.1021/bi991937j CCC: $19.00
Published on Web 01/14/2000

structural properties might constrain the energy landscapes for the folding of different proteins in the same family to the same path. This paper compares the folding mechanisms of two proteins, intestinal fatty acid binding protein (IFABP)[1] and ileal lipid binding protein (ILBP) from the intracellular lipid binding protein family (iLBPs). The iLBPs are a family of small hydrophobic ligand binding proteins (14−16 kDa, 127−136 amino acids) that function in the intracellular trafficking of small amphipathic ligands (*12*). These proteins have very similar structures, consisting of 10 antiparallel β-strands and 2 short α-helices (*13*), but differ in tissue distribution and ligand specificity (*12*, *13*). The β-strands are organized into two nearly orthogonal β-sheets surrounding a large internal ligand-binding cavity. Ligand binding has little effect on the overall structure of these proteins (*13*). None of these proteins have disulfide bonds, and all of the prolines are in the trans configuration in the native structures. Despite their similar structures, proteins in this family have degrees of sequence identity as low as 15% (data not shown). As such, these proteins are ideal for testing the hypothesis that proteins with similar structures but low degrees of sequence identity will have similar folding mechanisms.

No stable intermediates were detected by circular dichroism (CD), fluorescence, or absorbance measurements during the unfolding of several members of this family at equilibrium (*14*−*17*). However, stopped-flow fluorescence and CD experiments showed that at least one intermediate state was present on the unfolding and refolding pathways for several of these proteins (*14*−*20*).

MATERIALS AND METHODS

Protein Source and Purification. Recombinant IFABP was produced and isolated from *Escherichia coli* as previously described (*21*−*23*). Recombinant ILBP was found in the cytoplasm of *E. coli*, and was extracted from the cells using a French press (22, SLM Instruments). Following centrifugation to remove membranes and cellular debris, the supernatant was subjected to ammonium sulfate precipitation. The supernatant of a 60% ammonium sulfate fractionation was dialyzed against 20 mM Tris-HCl and 0.1 mM DTT (pH 8.0). The dialysate was loaded onto a Q Sepharose Fast Flow (Pharmacia) ion exchange column equilibrated with dialysis buffer and eluted with a linear gradient of 20 mM Tris-HCl, 50 mM NaCl, and 0.1 mM DTT (pH 8.0) to 20 mM Tris-HCl, 500 mM NaCl, and 0.1 mM DTT (pH 8.0). The fractions containing ILBP were concentrated using an Amicon concentrator and resolved on a G-50 Sephadex (Pharmacia) column equilibrated with 20 mM Tris-HCl, 5 mM NaN_3, and 0.1 mM DTT (pH 8.0). ILBP was delipidated as previously described (*24*). The protein purity was demonstrated by the presence of a single band on SDS−PAGE. An extinction coefficient of 0.87 mg^{-1} cm^{-1} at 280 nm was determined for ILBP (*25*).

Structural Alignment. The structures of pig ILBP (*26*) and rat IFABP (*27*) were aligned using the superimpose tool in the InsightII software suite (MSI Inc.), excluding insertions in either sequence. Pig ILBP is 71% identical and 88% homologous to rat ILBP, the protein used in this study. Since the structures of much more widely variant sequences in the iLBP family are similar, it is unlikely that there are any significant structure differences between pig ILBP and rat ILBP.

Reagents. Urea stock solutions (approximately 10 M) were prepared as previously described (*20*). Actual denaturant concentrations were determined by refractive index measurements with a Milton Roy Abbe-3C refractometer at 25 °C (*28*). All solutions contained 75 mM NaCl, 0.1 mM EDTA, and 25 mM NaH_2PO_4 (pH 8.0) and were filtered through a 0.22 μm membrane. DTT (0.1 mM) was added to the urea and buffer solutions immediately before use in experiments involving ILBP. Unless otherwise denoted, all chemicals were reagent grade.

Equilibrium Studies. Unfolding transitions were monitored by circular dichroism and fluorescence spectroscopy as a function of denaturant concentration. A Jasco J-710 spectropolarimeter was used to follow the change in secondary structure in the far-UV portion of the spectrum using a thermostated 0.1 mm cell at 25 °C. Fluorescence changes were followed with an Aminco-Bowman Series 2 luminescence spectrometer with excitation at 290 nm (2 nm band-pass) and emission at 327 nm (8 nm band-pass) in a 1 cm thermostated cell at 25 °C.

Nonlinear least-squares fits to the equilibrium data were generated by using KaleidaGraph (Synergy Software) in conjunction with an equation adapted from Santoro and Bolen (*29*) as previously described (*14*, *20*). All fits were to a minimum of two independent data sets.

Integrated Stopped-Flow Fluorescence Kinetic Studies. The kinetics of both unfolding and refolding were followed by fluorescence using an Applied Photophysics DX-17MV stopped-flow spectrophotometer. Excitation was at 290 nm (2 nm band-pass) using a 0.2 cm path length. The emission intensity was monitored above 305 nm at 90° through a WG305 Schott glass filter (Oriel) at 25 °C. Five parts of denaturant solution were mixed with 1 part of protein solution. For each urea concentration, five to seven transients were averaged. The dead time for this instrument was determined to be 5−10 ms (*20*). Data collected in this range were discarded from the analysis. The program supplied by Applied Photophysics was used to determine the nonlinear least-squares fit of the integrated fluorescence kinetic data to monophasic, monophasic plus steady state, and biphasic decay equations (*20*). Published criteria were used to determine the goodness of fit to the various models (*20*, *30*, *31*).

CD Kinetic Studies. The kinetics of unfolding and refolding of ILBP and IFABP were monitored with the Jasco J-710 spectropolarimeter using an RX1000 stopped-flow apparatus (Applied Photophysics) as previously described (*20*). Five parts of denaturant was mixed with one part of protein, and intensity changes were monitored at 218 nm. Five to seven transients were averaged for each final concentration of urea. Fitting was carried out as described above for stopped-flow fluorescence.

Fluorescence Spectral Kinetic Studies. The Applied Photophysics DX-17MV stopped-flow apparatus was adapted for the study of time-dependent fluorescence spectral changes

[1] Abbreviations: CD, circular dichroism; iLBPs, intracellular lipid binding proteins; ILBP, ileal lipid binding protein; IFABP, intestinal fatty acid binding protein; ΔG_{H_2O}, free energy of unfolding in the absence of denaturant; rmsd, root-mean-square difference; CRABP I, cellular retinoic acid binding protein I; CRBP II, cellular retinol binding protein II.

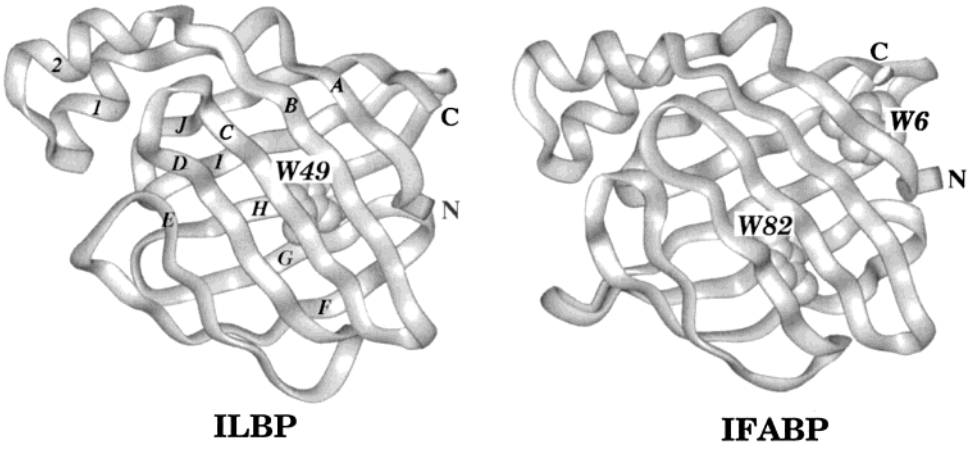

FIGURE 1: Ribbon drawing showing the backbone tracing and sequence location of the tryptophans of ILBP and IFABP. The strands and helices are labeled on the ILBP structure.

by replacing the WG305 cutoff filter with a high-efficiency monochromator (*20*). The excitation wavelength was 290 nm (9 nm band-pass). Kinetic time courses of the change in intensity during unfolding or refolding were collected for each 10 nm interval (9 nm band-pass) over a wavelength range from 310 to 400 nm. Five to seven transients were averaged at each wavelength. For both unfolding and refolding experiments, 5 parts of denaturant was mixed with 1 part of protein solution (0.52 mg/mL, final concentration). Final urea concentrations were 5.06, 5.88, and 6.73 M for unfolding and 1.05 and 2.01 M for refolding experiments. Extensive controls were performed using the reaction of *N*-acetyltryptophanamide with *N*-bromosuccinimide in urea to confirm the correct operation of the instrument and to ensure that no mixing artifacts were present (*20*).

GLint software (Applied Photophysics) was used to globally fit the kinetic spectral data (*20*). This program allows the entry of models that describe potential reaction mechanisms and optimizes the kinetic rates and amplitudes that describe the transition at each wavelength by nonlinear least-squares regression. The program produces goodness-of-fit parameters and residual plots of the kinetic data at all wavelengths and times to assess the accuracy of the model.

Fluorescence Double-Jump Kinetic Studies. The Applied Photophysics DX-17MV stopped-flow system was adapted to carry out sequential stopped-flow mixing. Excitation was at 290 nm, and the emission intensity was monitored above 305 nm as described above. Five parts of buffer solution was mixed with 1 part of unfolded protein in 7 M urea (initiating folding) and the mixture held in a 115 μL aging loop. Denaturant from a second set of syringes was mixed with the solution from the aging loop at a ratio of 7:2 after specific delay times and injected into the observation cell (initiating unfolding). For each time delay, five to seven transients were collected and fit to equations for monophasic and biphasic transitions. The average and standard deviation of the rates for each delay time are shown. Data collected during the dead time of the instrument (35 ms) were eliminated from the analysis. These experiments were less reproducible than the single-jump experiments described above, due to technical difficulties associated with multiple mixing events. The refolding time in the delay loop had to be limited to less than 20 s to avoid artifacts associated with the slow mixing of solutions in the delay loop.

Simulations of Protein Folding and Unfolding. KINSIM (*32*) was used to simulate the rates and amplitudes expected for the double-jump unfolding experiments described above. The simulations were based on a simple model for folding having one intermediate state.

Scheme 1

$$U \xrightarrow{k_1} I \xrightarrow{k_2} N$$

where k_1 is the rate for the formation of I from U and k_2 is the rate of formation of N from I. The rates for the folding reaction in the delay loop were calculated from the data shown in Figure 5, assuming that the folding rates show a logarithmic dependence on urea concentration (*33*).

$$\ln k_{[D]} = \ln k_{[0]} + (m_k/RT)[D]$$

where $k_{[D]}$ is the folding rate at some denaturant concentration, $k_{[0]}$ is the rate for that step at 0 M denaturant, m_k/RT is the slope from a plot of ln $k_{[D]}$ versus [D], and [D] is the denaturant concentration.

In the case of ILBP, k_1, k_2, and the amplitudes of the refolding phases were known from the single-jump experiments. The population of each state was calculated for any refolding time from these parameters. For IFABP, k_1 is not known, because the intermediate state is formed very rapidly or this rate is masked by the presence of a burst phase during refolding. However, k_2 is known, and the population of the native state was predicted from this rate for any refolding time.

RESULTS

Structure and Sequence Comparison. The structures of ILBP and IFABP were markedly similar (Figure 1), considering that only 23% of their residues are identical with an additional 16% that are similar (Figure 2). Alignments, including additional family members, showed that no residues are identical at any sequence location (data not shown). The rmsd for the superimposed backbone atoms for 123 of 127 residues of ILBP and IFABP was 1.98 Å. The excluded residues are shaded gray in Figure 2, and correspond to the insertion of an additional glycine between strands βC and βD, a deletion between strands βG and βH, and the addition of a C-terminal alanine for the sequence of ILBP compared

```
Structure    <====ßA====><===αI==>   <==αII==>  <==ßB==>  <==ßC==>   <===ßD==>
Rat IFABP    AFDGTWKVYRNENYEKFMEKMGINVVKRKLGAHDNLKLTITQEGNKFTVKESSN-FRNIDVVFELGVD
Rat ILBP     AFTGKYEFESEKNYDEFMKRLGLPDEVIERGRNFKIITEVQQDGENFTWSQSYSGGNIMSNKFTIGKE
Homology     ** * ..    .**..**...*.     . * .  .   . *.*  **  .* .    .   * .* .

Structure    <=ßE=>  <===ßF===>  <===ßG===>  <===ßH===>  <==ßI==>  <===ßJ===>
Rat IFABP    FAYSLADGTELTGTWTMEGNKLVGKFKRVDNGKELIAVREISGNELIQTYTYEGVEAKRIFKKE-
Rat ILBP     CEMQTMGGKKFKATVKMEGGKVVADFP------NYHQTSEVVGDKLVEISTIGDVTYERVSKRVA
Homology           * .   *  *** *.*  *       .     *. *..*..  *   *  .*. *.
```

FIGURE 2: Structure-based sequence alignment of rat ILBP and rat IFABP. Asterisks and periods denote identical and similar residues, respectively. Residues that are highly conserved (present in >90% of all sequences) throughout the iLBP family are boxed. The gray shaded areas indicate residues that were excluded from the rmsd calculation. The sequence locations of the strands and helices are shown above the alignments.

to IFABP. For comparison, the rmsd between the coordinates for the Cα atoms from the X-ray- and NMR-derived structures of IFABP was 2.3 Å (*34*).

Spectral Comparison. The CD spectra of the unfolded proteins were identical (data not shown). The CD spectra of the native proteins were similar in shape and intensity, but the spectrum of native ILBP was blue shifted with a minimum at 214 nm in comparison to a minimum at 217 nm for IFABP. Minima in this range reflect the extensive β-sheet structure in these proteins (*35*, *36*).

Differences in the fluorescence spectra were observed for these proteins in both the native and denatured state (data not shown). The shapes of the spectra were identical for the denatured proteins with a wavelength maximum at 352 nm, suggesting that the tryptophans of these proteins were equally exposed to solvent in the unfolded state. As expected, the fluorescence intensity of unfolded ILBP was half of that of unfolded IFABP, since IFABP has two tryptophans whereas ILBP has only one. The spectrum of native ILBP had a maximum at 342 nm in comparison to 334 nm for IFABP, indicating that the single tryptophan of ILBP was in a more polar environment than those of IFABP in the native state (*37*).

Equilibrium Studies. The unfolding of ILBP and IFABP at equilibrium with urea as the denaturant was monitored by CD and fluorescence (Figure 3). Data collected by both optical methods fit best to a simple two-state model. All unfolding transitions were completely reversible and showed no protein concentration dependence (data not shown). ILBP was less stable than IFABP with a midpoint for denaturation of 2.9 M urea compared to 4.0 M urea for IFABP. The free energies of unfolding in the absence of urea (ΔG_{H_2O}) for IFABP were similar as determined by fluorescence (5.28 ± 0.56 kcal mol^{-1}) and CD (5.86 ± 0.43 kcal mol^{-1}). Somewhat lower ΔG_{H_2O} values were determined for ILBP by CD (4.39 ± 0.26 kcal mol^{-1}) and fluorescence (4.71 ± 0.27 kcal mol^{-1}). The transitions monitored at other wavelengths by both methods were virtually identical. Since the data fit well to a two-state model, it appeared that only the native and fully denatured forms of ILBP and IFABP were present at equilibrium by these techniques.

Unfolding Kinetic Studies. A typical transition for the unfolding of ILBP as monitored by stopped-flow fluorescence is shown in Figure 4. The total change in intensity at wavelengths greater than 305 nm was observed. These experiments are termed stopped-flow integrated fluorescence, to differentiate them from the stopped-flow fluorescence spectral studies. The transition was biphasic, as shown by

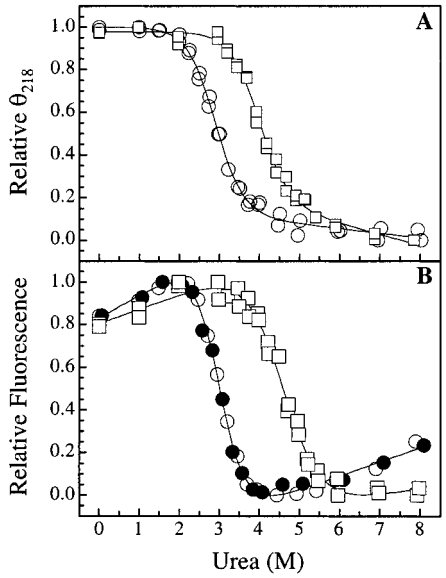

FIGURE 3: Unfolding of ILBP (○) and IFABP (□) at equilibrium monitored by (A) CD and (B) fluorescence at 340 nm. The final protein concentrations were 100 μg/mL for CD and 10 μg/mL for fluorescence. The reversibility of ILBP (●) by fluorescence is shown. Lines depict the fit to a two-state model.

the improvement in the fit of the data to a biexponential equation. Two rates were detected during the unfolding of ILBP at all final concentrations of urea (Figure 5). However, unfolding transitions observed by stopped-flow CD were best fit by a single-exponential equation at each urea concentration. The rate detected by CD was identical to the slower of the two rates detected by fluorescence (Figure 5). The initial and final optical signals at a variety of denaturant concentrations were used to construct equilibrium unfolding plots for the stopped-flow instruments (Figure 6). Fits of these data to a simple two-state model for the unfolding transition resulted in ΔG_{H_2O} and denaturation midpoint values that were within error of those stated above. These plots were used to calculate the expected amplitude change for any folding or unfolding transition, assuming a linear dependence of fluorescence intensity of the folded and unfolded states on denaturant concentration. The entire expected amplitude change for unfolding transitions was observed by both CD and fluorescence. Approximately 15−20% of the expected amplitude change was associated with the faster rate of unfolding with the remaining 80−85% of the total amplitude change attributed to the slower rate.

During the unfolding of IFABP, two rates were observed by integrated stopped-flow fluorescence (*17*, *20*). The entire

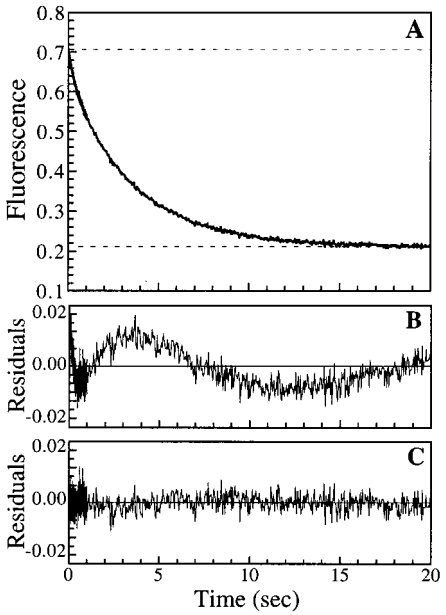

FIGURE 4: (A) Change in the integrated fluorescence intensity vs time for the unfolding of ILBP. The final concentrations of urea and protein were 6.2 M and 0.26 mg/mL, respectively. The dashed lines are the values expected for completely folded and unfolded ILBP under these conditions. The residuals of the fit to (B) monophasic and (C) biphasic relaxation equations are shown.

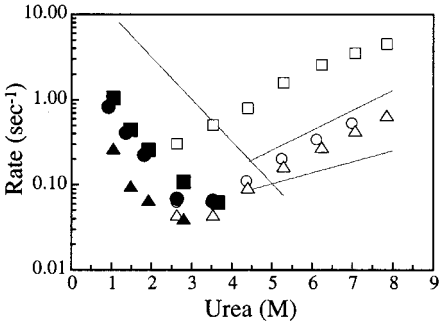

FIGURE 5: Folding (■, ▲, and ●) and unfolding (□, △, and ○) rates of ILBP observed by stopped-flow CD (circles) and stopped-flow integrated fluorescence (squares and triangles). The final protein concentration was 0.52 mg/mL for CD and 0.26 mg/mL for fluorescence. The lines show the comparable rates for unfolding and refolding by fluorescence for IFABP. The rates observed by CD for IFABP were identical to the faster rates observed by fluorescence.

expected amplitude change was observed (Figure 6B). Unlike ILBP, 75−80% of the expected amplitude change by fluorescence was attributed to the faster phase with the remainder occurring at the slower rate. Only one rate was detected by CD which coincided with the faster of the two fluorescence rates and accounted for the entire expected CD amplitude change. A slower rate with as little as 10% of the total CD amplitude change would have been detected if present (*20*). The rates for the unfolding of IFABP are shown as lines in Figure 5.

Refolding Kinetic Studies. Figure 7 shows a typical experiment in which the refolding of ILBP is monitored by integrated stopped-flow fluorescence. These data were best fit by a double-exponential equation at each final urea concentration during folding. The entire expected amplitude change was observed (Figure 6A). The faster rate accounted for approximately 80% of the expected fluorescence amplitude change, with about 20% of the expected amplitude

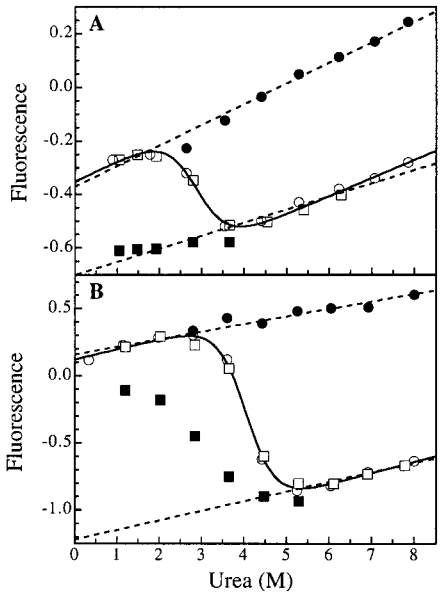

FIGURE 6: Fluorescence signals obtained from unfolding (○ and ●) and refolding (□ and ■) stopped-flow integrated fluorescence for (A) ILBP and (B) IFABP. Filled symbols are for the initial fluorescence signal at the start of the kinetic transition, and open symbols are for the fluorescence signal at the end of the experiment. The dashed lines indicate the expected fluorescence intensity of the native and unfolded proteins based on the linear regression of the native and unfolded baselines. The solid line is the fit of the data depicted by the open symbols to a two-state model for the unfolding transition.

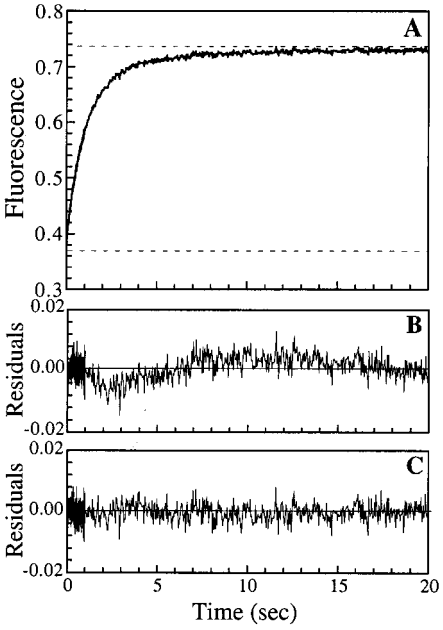

FIGURE 7: (A) Change in the integrated fluorescence intensity vs time for the refolding of ILBP. The final concentrations of urea and protein were 1.05 M and 0.26 mg/mL, respectively. The dashed lines are the values expected for completely folded and unfolded ILBP under these conditions. The residuals of the fit to (B) monophasic and (C) biphasic relaxation equations are shown.

change attributed to the slower rate. The amplitudes of these phases were independent of final urea concentration. The faster of the observed folding rates corresponded to the single rate observed by CD for the same transition (Figure 5). The entire expected amplitude change was observed by CD.

During the folding of IFABP, a single phase was observed by both fluorescence and CD at identical rates (*17*, *20*). The

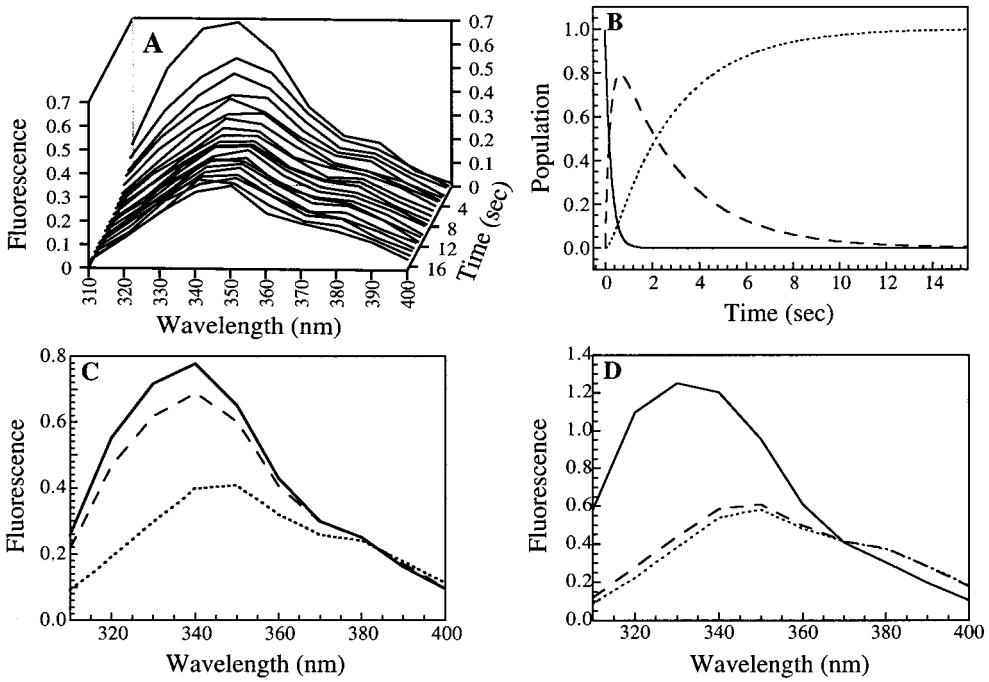

FIGURE 8: (A) Time-resolved fluorescence spectra for the unfolding of ILBP at final concentrations of 6.77 M for urea and 0.83 mg/mL for protein. Unfolding was initiated by mixing 1 part of native protein (5 mg/mL) in buffer with 5 parts of a 8.12 M urea solution in buffer. Two percent of the total collected data are shown as spectral slices at specific times after the initiation of unfolding. (B) The time-dependent concentrations of the native (solid line), intermediate (dashed line), and denatured (dotted line) states from the fit of the data to the model N ⇒ I ⇒ U. (C) The fluorescence spectra of the native (solid line), intermediate (dashed line), and unfolded (dotted line) states of ILBP during unfolding. (D) The fluorescence spectra of the native (solid line), intermediate (dashed line), and unfolded (dotted line) states of IFABP during unfolding (final concentrations of 0.52 mg/mL for protein and 7.7 M for urea).

folding of IFABP was 5-fold faster than that of ILBP. Amplitude analysis showed the presence of a burst phase during the folding of IFABP by both optical methods (Figure 6B). Unlike ILBP, the amplitudes associated with the burst and observed phases for IFABP were dependent on the final urea concentration. As the final concentration of denaturant decreased, the amplitude of the burst phase increased and the amplitude of the observed phase decreased (Figure 6B). The rates for the refolding of IFABP are shown as a line in Figure 5.

Wavelength-Dependent Stopped-Flow Fluorescence. To better characterize the properties of the intermediate states, the changes in the overall fluorescence spectra were determined during both the folding and unfolding process. The emission fluorescence intensities at specific wavelengths for the unfolding of ILBP are shown in Figure 8A. Transitions at individual wavelengths from 310 to 360 nm were best fit by a biexponential equation, with rate constants identical to the rates measured by stopped-flow integrated fluorescence for the same change in denaturant concentration. The simplest model that fit the data required an intermediate state on the unfolding pathway. An initial rise in the concentration of the intermediate occurred, followed by the appearance of unfolded ILBP after a short lag period (Figure 8B). The initial and final spectra were identical to those of native and denatured ILBP, respectively, in this instrument. The intermediate spectrum was similar to that of the native protein with somewhat less intensity (Figure 8C) and is different from the spectrum of the intermediate observed during the unfolding of IFABP, which was similar to that of the denatured protein (Figure 8D). The shoulder in these emission spectra at 380 nm is due to a monochromator artifact.

The emission fluorescence intensities at specific wavelengths during the refolding of ILBP are shown in Figure 9A. At individual wavelengths between 310 and 370 nm, the refolding transitions were monophasic with rates slightly slower than the faster rate measured by stopped-flow integrated fluorescence. The improvement in fit associated with a biexponential process was not significant. However, when the transitions for the individual wavelengths were summed in a manner analogous to the integrated stopped-flow fluorescence method, the resulting transition was biphasic with rates identical to those determined by the integrated method at that final concentration of denaturant. The global analysis of the intensity change at all wavelengths was best fit by a sequential model including a single intermediate. The changes in concentration for the various spectral states are shown in Figure 9B. The initial and final spectra were those expected for unfolded and native ILBP, respectively, at this final concentration of denaturant (Figure 9C). The spectrum of the intermediate state was very similar to that observed during the unfolding of ILBP (Figures 8C and 9C).

Very different results were observed for the folding of IFABP (Figure 9D; *20*). Transitions were monophasic with rates identical to those observed by CD and integrated fluorescence at all wavelengths. The initial spectrum was different from that of the denatured state, and blue shifted and more intense than that of the intermediate observed during unfolding. At lower urea concentrations, the initial spectrum became more and more native-like in appearance (*20*). The final spectrum was identical to that expected for native IFABP.

Double-Jump Experiments. Stopped-flow double jump methods (*38*) were used to further characterize the refolding

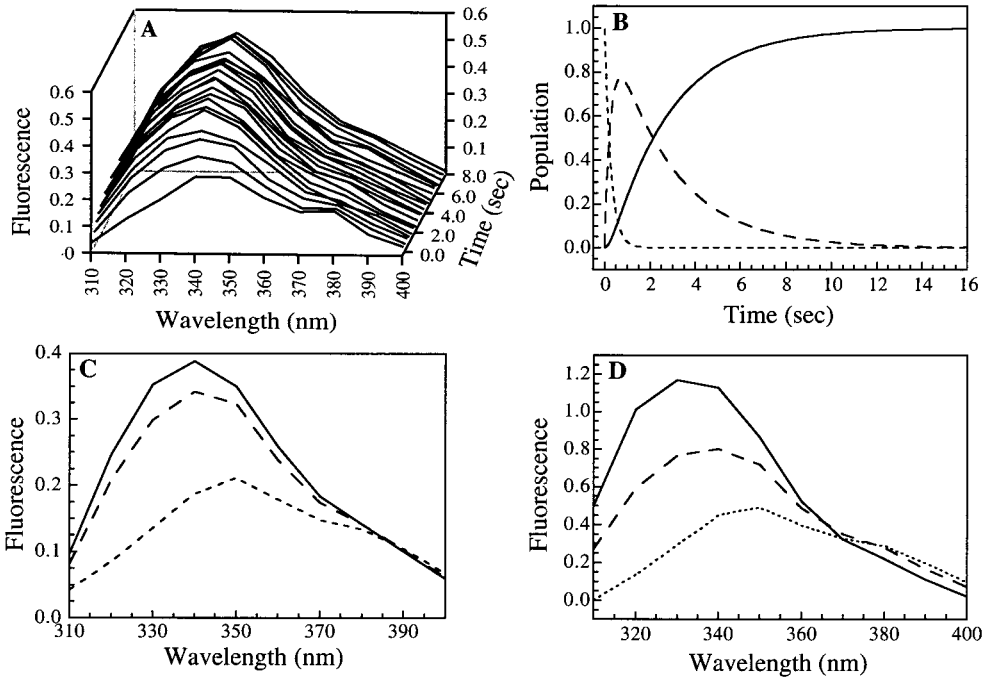

FIGURE 9: (A) Time-resolved fluorescence spectra for the refolding of ILBP at final concentrations of 1.04 M for urea and 0.83 mg/mL for protein. Refolding was initiated by mixing 1 part of unfolded protein (5 mg/mL) in 6.25 M urea with 5 parts of buffer. Two percent of the total collected data are shown as spectral slices at specific times after the initiation of refolding. (B) The time-dependent concentration of the native (solid line), intermediate (dashed line), and unfolded (dotted line) states from the fit of the data to the model U ⇒ I ⇒ N. (C) The fluorescence spectra of the native (solid line), intermediate (dashed line), and unfolded (dotted line) states are shown. (D) The fluorescence spectra of the native (solid line) and initial (dashed line) states of IFABP are shown with the spectra of the unfolded form of IFABP (dotted line).

pathway for these proteins. In these experiments, unfolded protein in urea was rapidly mixed with buffer to initiate refolding. After a defined period of time, the solution was mixed with a high concentration of urea to initiate unfolding, and the unfolding reaction was monitored by stopped-flow integrated fluorescence. The rate(s) and amplitudes of the refolding reaction were known from the single-mixing experiments described above. Assuming that these proteins follow a simple reversible mechanism with a single intermediate state present during the folding reaction,

Scheme 2

$$U \Leftrightarrow I \Leftrightarrow N$$

the expected populations of the native (N), intermediate (I), and unfolded (U) states could be calculated by simulation for any specified refolding time. These predicted concentrations were compared to the observed concentrations of these states as measured by the unfolding reaction. At very long delay times (sufficient to allow complete refolding), the rates and amplitudes observed during unfolding were identical to those from the single-mix unfolding experiments described above. At short refolding delay times, most of the protein is still unfolded, and the remainder will not have proceeded beyond the intermediate state. Therefore, only the rate for the conversion of the intermediate to the unfolded state should be observed at short refolding times (*39*).

In the case of ILBP, where all of the kinetic constants for the folding and unfolding reactions are known, the observed rates and amplitudes corresponded well to the values predicted from the simulations (Figure 10). As such, these experiments support the hypothesis that ILBP folds by a simple reversible mechanism with an on-path intermediate.

The presence of a burst phase during the refolding of IFABP complicated the interpretation of the double-jump experiments. The burst phase amplitude accounted for approximately 60% of the total expected amplitude change during refolding at this final concentration of denaturant. However, this burst phase signal during refolding did not exhibit a corresponding amplitude change during unfolding at short delay times. A second complication is that only one rate was observed during the refolding of IFABP, rather than the two rates expected for a reversible folding reaction of a protein having an intermediate on its folding pathway.

It was assumed that the single rate observed during refolding represents the rate of formation of native protein from the intermediate state, and that the rate of accumulation of the intermediate state was very rapid and/or masked by the burst phase. Since the rate of refolding to the native state was known from the single-mix experiments described above, the amount of native protein present could be predicted for each refolding time, and compared to the amplitude of the first observed unfolding phase (the N to I reaction). Thus, the measured amplitude of the first unfolding phase for a particular delay time divided by the amplitude change for this phase at long refolding delay times is the fraction of native protein present at that delay time. The close correspondence between the predicted and observed amplitude of the first phase supported this hypothesis (Figure 11B). The amplitude of the second phase observed during unfolding (the I to U reaction) was greater than that expected from the amount of native protein present at short refolding times (Figure 11B). This amplitude was converted to the fractional population of the intermediate state in Figure 11C. The simplest explanation for these data is that the intermediate

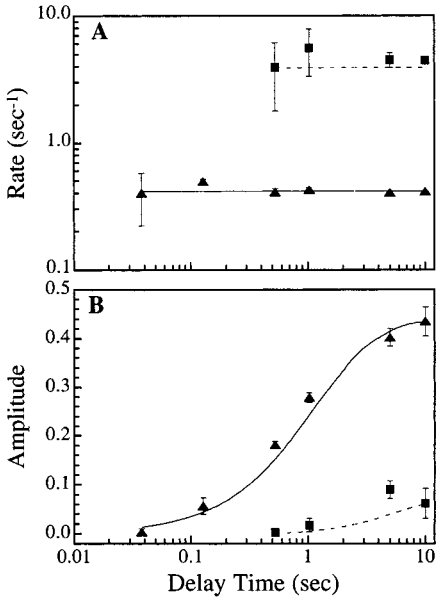

FIGURE 10: Double-jump unfolding of ILBP. One part of 5.52 mg/mL ILBP in 6.25 M urea was mixed with 5 parts of buffer to initiate refolding. The concentrations of urea and protein following this step were 1.05 M and 0.92 mg/mL, respectively. The predicted rates of folding at this final concentration of denaturant are 0.90 and 0.20 s^{-1}. Folding proceeded for the delay times shown, and the aged solution was mixed with 9.4 M urea (2:7 ratio) to initiate the unfolding reaction. The final concentrations of urea and protein after the second mix were 7.0 M and 0.26 mg/mL, respectively. (A) The observed rates are the average of at least four transients at each time delay for the faster (■) and slower (▲) phases. The error bars shown are one standard deviation and may be within the size of the symbol. The lines are the expected rates for the faster (dashed) and slower (solid) unfolding reaction at this final concentration of denaturant. (B) The observed amplitudes for the faster (■) and slower (▲) phases. The lines are the expected amplitudes for the faster (dashed) and slower (solid) unfolding reactions from simulation of a simple reversible mechanism for folding (N ⇔ I ⇔ U).

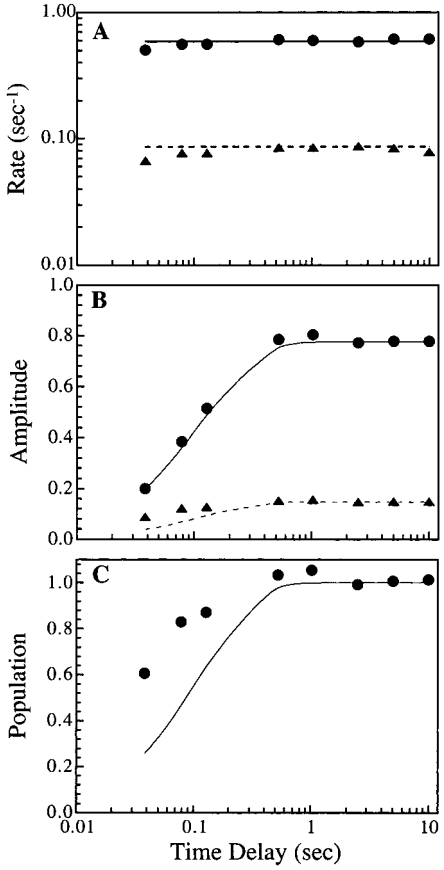

FIGURE 11: Double-jump unfolding of IFABP. One part of 5.52 mg/mL IFABP in 7.26 M urea was mixed with 5 parts of buffer to initiate refolding. The concentrations of urea and protein following this step were 1.21 M and 0.92 mg/mL, respectively. The predicted rate of folding at this final concentration of denaturant is 7.84 s^{-1}. Folding was allowed to proceed for the delay times shown, and the aged solution was mixed with 9.3 M urea (2:7 ratio) to initiate the observed unfolding reaction. The final concentrations of denaturant and protein after the second mix were 7.0 M and 0.26 mg/mL, respectively. (A) The observed rates are the average of at least four transients at each time delay for the faster (●) and slower (▲) phases. The error bars are within the size of the symbol. The lines are the expected rates for the faster (solid line) and slower (dashed line) unfolding reactions at this final concentration of denaturant. (B) The observed amplitudes for the faster (●) and slower (▲) phases. The lines are the expected amplitudes for the faster (solid line) and slower (dashed line) unfolding reactions from simulations. (C) The observed population of the intermediate state. The line represents the predicted population of the intermediate state assuming that it is formed only by the breakdown of the native protein during unfolding.

state observed during unfolding must accumulate prior to the production of native protein, suggesting that the intermediate observed during the unfolding of IFABP was on the refolding path as well, even though it could not be directly detected by single-jump experiments.

DISCUSSION

IFABP and ILBP are nearly ideal systems for the study of protein folding. IFABP has no cysteines or prolines, thereby avoiding the problems those residues can cause during refolding. ILBP has two prolines (in the trans configuration in the native state) and one cysteine in its sequence. Although ILBP and IFABP have very similar structures, the number and location of tryptophans in the two proteins are different. In IFABP, W6 is located on the N-terminal strand of the top β-sheet while W82 is found on the N-terminal strand of the bottom β-sheet (Figure 1). The sole tryptophan of ILBP (W49) is situated on the upper β-sheet in the middle of the third strand.

Equilibrium Studies. ILBP was significantly less stable than IFABP. Bile salts, the major ligands of ILBP, are both larger and more rigid than the fatty acids that IFABP binds (*10*, *23*). It has been suggested that the hydrogen bonding network in the β-sheet of ILBP may be less stable in comparison to those of other iLBPs that bind fatty acids. This destabilization may be necessary to make the overall structure of ILBP more flexible for it to bind bile salts (*26*). This additional flexibility did not affect the reversibility of unfolding of ILBP. Further, no significant populations of intermediates were detected at equilibrium by optical methods for either protein.

Folding Mechanism of ILBP. Most small, single-domain proteins exhibit monophasic kinetics during unfolding (*40*). However, this is not the case for any of the iLBPs examined thus far (*14*, *16*, *17*, *20*). These proteins exhibit biphasic unfolding kinetics by fluorescence and monophasic unfolding kinetics by CD. The kinetic model that best fit the unfolding data is

Scheme 3

$$N \Rightarrow I \Rightarrow U$$

where N, I, and U stand for the native, intermediate, and unfolded states, respectively.

During the unfolding of ILBP a small amplitude change was associated with the faster rate observed by fluorescence (the N to I step). The majority of the fluorescence and all of the CD amplitude change occurred at a slower rate (the I to U step). As such, this intermediate appears to have retained all of its secondary structure. The fluorescence spectrum of the intermediate was similar to that of native ILBP but with a slightly lower intensity (Figure 8C), suggesting that the local environment of the tryptophan was as hydrophobic in the intermediate state as in the native state. Thus, the unfolding intermediate of ILBP was molten globule-like (*41*); it had native-like secondary structure, and the hydrophobic core in the vicinity of W49 was not exposed to solvent.

The refolding of ILBP was characterized by a biphasic recovery of the native state fluorescence. A simple model that fit the data well is shown here:

Scheme 4

$$U \rightleftharpoons I \rightleftharpoons N$$

The first observed phase accounted for the entire CD and most of the expected fluorescence amplitude change. Therefore, the first step in the folding of ILBP resulted in an intermediate that had recovered all of its secondary structure and most of its fluorescence.

Slow folding reactions are frequently caused by proline isomerization. Varying the amount of time ILBP was in the completely unfolded state from 30 s to 3 h did not change the amplitudes or rates of refolding (data not shown), as would be expected for a proline isomerization-dependent reaction (*42*). The slower rate of refolding was highly dependent on urea concentration, which is not the case for most proline isomerization-dependent transitions (*42*). The rate of refolding was unusually rapid for proline isomerization (extrapolated rate of 1.44 s^{-1} at 0 M urea), which are normally slower than 0.1 s^{-1} (*42*). Finally, addition of human cyclophilin during refolding under solvent conditions similar to those used to accelerate the folding of chymotrypsin inhibitor protein II (*43*) did not change the observed rates or amplitudes during the folding of ILBP. As such, it seems unlikely that proline isomerization was important in the folding of ILBP.

This intermediate state was not an artifact caused by multiple slowly exchanging native forms of the protein, since none were detected by NMR (*26*). This state was not caused by transient aggregation (*44*), since varying the protein concentration over a 7-fold range (8−60 μM) did not change the rates or relative amplitudes of any of the observed phases. All of the experiments reported here were carried out in this concentration range. Higher final protein concentrations (>70 μM) did show an additional small amplitude slower phase that might be the result of aggregation.

The fluorescence spectral properties of this refolding intermediate were nearly identical to those of the intermediate observed during unfolding, suggesting that ILBP follows a simple reversible folding mechanism:

Scheme 5

$$U \leftrightharpoons U \leftrightharpoons N$$

The nearly perfect correlation between predicted and measured rates and amplitudes in the double-jump unfolding experiments supported this hypothesis. Thus, the intermediate was on path and has the structural properties of a molten globule.

Folding Mechanism of IFABP. In contrast, the intermediate observed during the unfolding of IFABP was not a molten globule, since it had little if any secondary structure as determined by CD. The fluorescence spectrum of this intermediate was similar to that of unfolded IFABP, although it was slightly blue shifted and slightly more intense. This structure possessed some tertiary contacts that were the first to form during folding and the last to break down during unfolding. Proton NMR studies at equilibrium, under solution conditions resulting in completely unfolded structures by optical methods, have shown the presence of local and nonlocal hydrophobic tertiary contacts in 434 repressor (*45*), bovine pancreatic trypsin inhibitor (*46*−*48*), and the α-subunit of tryptophan synthase (*49*). Previous studies of the equilibrium unfolding of 6-fluorotryptophan-labeled IFABP by ^{19}F NMR have shown that tryptophan 82 is involved in a structure that appears to be completely unfolded by optical techniques (*15*). The kinetic intermediate observed during the unfolding of IFABP may be similar to these NMR-detected structures.

The folding of IFABP was also different from that of ILBP (*20*). A burst phase was detected by both CD and fluorescence. The product of the burst phase has considerably more secondary structure and was much more fluorescent than the unfolded state. The CD and fluorescence spectra of the burst phase product were not that of the molten globule form observed at low pH for IFABP, which is not on a productive folding path (*17*). The double-jump experiments showed that the burst phase state had no corresponding unfolding reaction. Hydrogen exchange experiments showed no protection of amide hydrogens during the burst phase (data not shown), suggesting that any hydrogen bonds made during the burst phase were not stable. No amide hydrogen protection was observed early in the folding of another member of this family, cellular retinoic acid binding protein I (CRABP I; *14*). This burst phase may represent the formation of a collapsed denatured state, in rapid equilibrium with the extended unfolded state. At low concentrations of denaturant, the collapsed denatured state is the favored unfolded form of the protein. At high concentrations of denaturant, the fully extended form is favored. This state would be similar to those postulated for cytochrome *c* (*50*, *51*) and ribonuclease A (*52*).

Only one identical rate was observed by CD and fluorescence during the folding of IFABP. Normally, two phases would be observed for folding reactions involving an intermediate. However, if the first step (U to I) is rapid compared to the dead time of the instrument (*53*), or if it is masked by the burst phase described above, only the second slower phase would be observed. The double-jump experiments supported this hypothesis. The following mechanism is the simplest model for the folding of IFABP:

Scheme 6

$$D \leftrightharpoons U \leftrightharpoons I \leftrightharpoons N$$

where N, I, U, and D stand for the native, intermediate,

extended unfolded, and collapsed denatured states, respectively.

It is unlikely that multiple native forms of IFABP were responsible for the unfolding kinetics since none were observed by NMR (*34*). Proline isomerization is not involved in the folding of IFABP since no prolines are found in its sequence (Figure 2). Protein aggregation did not appear to be involved in these processes since no dependence of the reaction rates or amplitudes on protein concentration was observed over a 20-fold concentration range (4−80 μM).

The model described here is the simplest that fit the data for the folding of IFABP. More complex models could describe the data as well. There may be a direct link between the D state and the I state, placing the D state on path, but the data cannot discriminate between these models.

Hypothesis about the Differences in the Mechanism of Folding. Despite having such similar native structures, the intermediates on the folding paths of ILBP and IFABP have very different spectral and structural characteristics. Similar results have been found for two other proteins in this family, CRABP I and cellular retinol binding protein II (CRBP II). The folding of CRABP I is similar to that of ILBP, and the folding of CRBP II is similar to that of IFABP (*16*). As such, it appears that there are at least two routes to formation of the iLBP fold, and that different sequences have a preference for one of these routes. The intermediates are unlikely to be a single-conformation state. They are probably an ensemble of structures having a similar structural core for a limited number of residues, with the other residues having many different conformations. This is particularly true for the intermediate observed during the folding of IFABP and CRBP II, since no stable secondary structure was present.

One potential explanation for these results may be related to the location of the tryptophans in the two proteins. Intermediates can only be detected by stopped-flow fluorescence if their structure contains a reporting group. The sole tryptophan of ILBP (Trp49) is situated in a different structural position in comparison to the two tryptophans (Trp6 and Trp82) of IFABP (Figure 1). Therefore, a tryptophan at the Trp49 structural location may be necessary to detect a molten globule-like intermediate. If a single tryptophan is put into IFABP at a position structurally homologous to that found in ILBP, a molten globule-like intermediate might be detected for IFABP as well. Studies of mutant proteins have shown that only Trp82 was involved in the kinetic intermediate observed for IFABP (unpublished data). As such, placement of a tryptophan at a position in ILBP structurally homologous to that of Trp82 in IFABP may lead to the detection of an intermediate similar to that observed for IFABP. However, site-directed mutagenesis has been used to place tryptophans at identical locations in the structures of CRABP I and CRBP II. The location of the optical probes did not affect the observed kinetic mechanisms in these proteins (data not shown). As such, this hypothesis seems unlikely to be the cause of the observed differences in the mechanism of folding.

An alternative explanation involves the energetics of the unfolding process. A limitation of stopped-flow methods is that an intermediate must accumulate to significant concentrations to be directly observed. Consider the possibility that these proteins must pass through two different intermediate states to arrive at the native structure.

Scheme 7

$$U \rightleftharpoons I_1 \rightleftharpoons I_2 \rightleftharpoons N$$

The first of these intermediates, I_1, is the intermediate which lacks secondary structure like that observed during the folding of IFABP. The second intermediate, I_2, is the molten globule-like intermediate observed during the folding of ILBP. I_1 accumulates during the folding of IFABP and thus is observed, but I_2 is not sufficiently stable to accumulate and is not detected. During the folding of ILBP, I_1 does not accumulate and is not detected, but I_2 is stable and observed. Although the same overall folding path is being followed by both proteins, intermediate states with different spectral properties and different structures are detected. Different solvent conditions (pH, temperature, and denaturants) may modulate the stability of intermediates, allowing them to be detected. This thermodynamic stability hypothesis for the folding process represents a simple one-dimensional energetic landscape for protein folding.

Finally, it may be that the folding mechanisms for these proteins are truly different from each other. In this case, the differences in sequence of these proteins are sufficient to dictate different paths from the native state to the unfolded state and vice versa, perhaps by differences in residual structure in the unfolded state or by different nucleation sites, and are consistent with the landscape model for protein folding (*2*).

Physical Basis for the Differences in the Folding Mechanism. Although these results favor the landscape model for folding, the kinetic data do not indicate the physical basis for the observed results. There are no significant differences in topology or total burial of hydrophobic surface among these proteins. However, the structures of these proteins differ somewhat in the location of the buried hydrophobic residues, and the degree of hydrophobicity of these buried clusters. The hydrophobic core of these proteins is located opposite the α-helices, between the two β-sheets (Figure 12). A greater number of hydrophobic atoms are found in this cluster for IFABP (50 atoms) than for ILBP (33 atoms). The increased hydrophobicity in this region may be the reason that a state lacking stable secondary structure was detected for IFABP. The less hydrophobic core of ILBP may cause this state to be less stable, and thus not detectable by stopped-flow methods.

Note that the residues that participate in this cluster come from several strands of both top and bottom β-sheets. If this tertiary hydrophobic cluster is the initial site of structure formation in these proteins, a template for the final hydrogen bonding network would be present, since the reverse turns necessary to make the correct secondary structure must be present at approximately the correct locations to make this cluster. Additional evidence for this type of initiating state was found by ^{19}F NMR studies of the folding of IFABP (*15*). This is a very attractive mechanism for the formation of β-sheet structure, where hydrophobic contacts between residues that are distant in the amino acid sequence may simplify the search for the final structure of the protein (*54*).

In summary, ILBP was less stable than IFABP and had a molten globule-like intermediate on both its unfolding and refolding pathway. IFABP, on the other hand, had an intermediate with no secondary structure on its folding

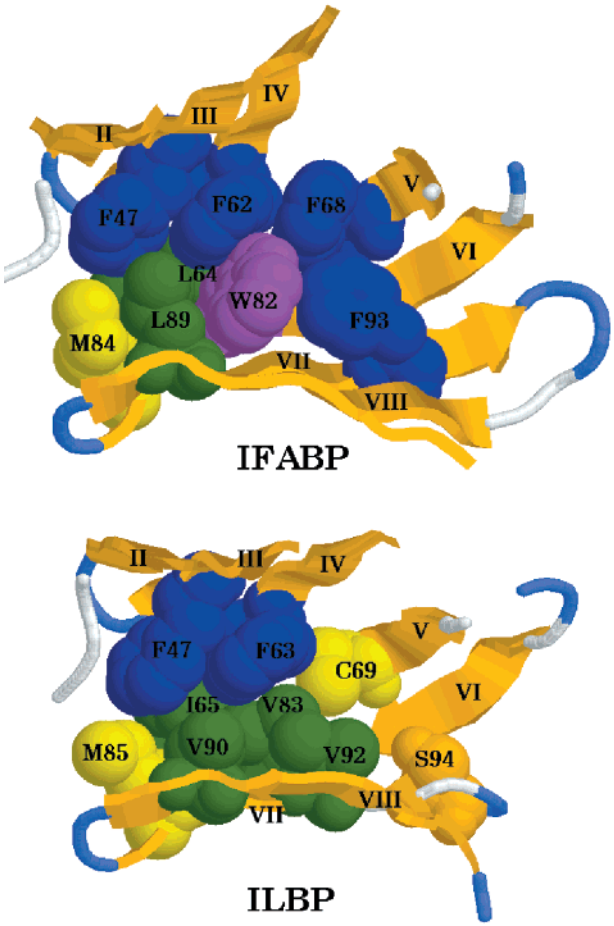

FIGURE 12: Hydrophobic clusters of IFABP and ILBP. The β-strands of the top sheet (II−VI) and bottom sheet (VI−VIII) are labeled. Hydrophobic residues within 7.5 Å of W82 in IFABP and V83 in ILBP are shown and labeled. The view is looking between the sheets with the α-helices projecting toward the viewer (see Figure 1). The helices and parts of the sheets have been removed so that the core can be viewed. Almost all of the atoms in these side chains are completely excluded from solvent in both structures.

pathway. These results show that dissimilar sequences can have different energetic routes to the same final structure.

ACKNOWLEDGMENT

We thank Dr. D. Cistola, Dr. C. Frieden, Dr. G. Rose, Dr. E. Lattman, Dr. D. Shortle, and Dr. C. R. Matthews for helpful discussions.

REFERENCES

1. Levinthal, C. (1968) *J. Chim. Phys. 65*, 44−45.
2. Dill, K. A., and Chan, H. S. (1997) *Nat. Struct. Biol. 4*, 10−19.
3. Shakhnovich, E., Abkevich, V., and Ptitsyn, O. (1996) *Nature 379*, 96−98.
4. Michnick, S. W., and Shakhnovich, E. (1998) *Folding Des. 3*, 239−251.
5. Ptitsyn, O. B. (1998) *J. Mol. Biol. 278*, 655−666.
6. Martinez, J. C., Pisabarro, M. T., and Serrano, L. (1998) *Nat. Struct. Biol. 5*, 721−729.
7. Lang, K., Wrba, A., Krebs, H., Schmid, F. X., and Beintema, J. J. (1986) *FEBS Lett. 204*, 135−139.
8. Stackhouse, T. M., Onuffer, J. J., Matthews, C. R., Ahmed, S. A., and Miles, E. W. (1988) *Biochemistry 27*, 824−832.
9. Hooke, S. D., Radford, S. E., and Dobson, C. M. (1994) *Biochemistry 33*, 5867−5876.
10. Kragelund, B. B., Hojrup, P., Jensen, M. S., Schjerling, C. K., Juul, E., Knudsen, J., and Poulsen, F. M. (1996) *J. Mol. Biol. 256*, 187−200.
11. Perl, D., Welker, C., Schindler, T., Schroder, K., Marahiel, M. A., Jaenicke, R., and Schmid, F. X. (1998) *Nat. Struct. Biol. 5*, 229−235.
12. Bass, N. M. (1993) *Mol. Cell. Biochem. 123*, 191−202.
13. Banaszak, L., Winter, N., Xu, Z., Bernlohr, D. A., Cowan, S., and Jones, T. A. (1994) *Adv. Protein Chem. 45*, 89−151.
14. Ropson, I. J., Gordon, J. I., and Frieden, C. (1990) *Biochemistry 29*, 9591−9599.
15. Ropson, I. J., and Frieden, C. (1992) *Proc. Natl. Acad. Sci. U.S.A. 89*, 7222−7226.
16. Burns, L. L., Dalessio, P. M., and Ropson, I. J. (1998) *Proteins: Struct., Funct., Genet. 33*, 107−118.
17. Dalessio, P. M., and Ropson, I. J. (1998) *Arch. Biochem. Biophys. 359*, 199−208.
18. Clark, P. L., Liu, Z. P., Zhang, J., and Gierasch, L. M. (1996) *Protein Sci. 5*, 1108−1117.
19. Clark, P. L., Liu, Z. P., Rizo, J., and Gierasch, L. M. (1997) *Nat. Struct. Biol. 4*, 883−886.
20. Ropson, I. J., and Dalessio, P. M. (1997) *Biochemistry 36*, 8594−8601.
21. Lowe, J. B., Sacchettini, J. C., Laposata, M., McQuillan, J. J., and Gordon, J. I. (1987) *J. Biol. Chem. 262*, 5931−5937.
22. Sacchettini, J. C., Gordon, J. I., and Banaszak, L. J. (1989) *J. Mol. Biol. 208*, 327−339.
23. Sacchettini, J. C., Banaszak, L. J., and Gordon, J. I. (1990) *Mol. Cell. Biochem. 98*, 81−93.
24. Glatz, J. F. C., and Veerkamp, J. H. (1983) *Anal. Biochem. 132*, 89−95.
25. Pace, C. N., Vajdos, F., Fee, L., Grimsley, G., and Gray, T. (1995) *Protein Sci. 4*, 2411−2423.
26. Lücke, C., Ahang, F., Ruterjans, H., Hamilton, J. A., and Sacchettini, J. C. (1996) *Structure 4*, 785−800.
27. Scapin, G., Gordon, J. I., and Sacchettini, J. C. (1992) *J. Biol. Chem. 267*, 4253−4269.
28. Pace, C. N. (1986) *Methods Enzymol. 131*, 266−280.
29. Santoro, M. M., and Bolen, D. W. (1988) *Biochemistry 27*, 8063−8068.
30. Mannervik, B. (1982) *Methods Enzymol. 87*, 370−389.
31. Motulsky, H. J., and Ransnas, L. A. (1987) *FASEB J. 1*, 365−374.
32. Frieden, C. (1994) *Methods Enzymol. 240*, 311−323.
33. Park, S. H., O'Neil, K. T., and Roder, H. (1997) *Biochemistry 36*, 14277−14283.
34. Hodsdon, M. E., and Cistola, D. P. (1997) *Biochemistry 36*, 1450−1460.
35. Johnson, W. C. (1988) *Annu. Rev. Biophys. Biophys. Chem. 17*, 481−507.
36. Woody, R. W. (1995) *Methods Enzymol. 246*, 34−71.
37. Permyakov, E. A. (1993) *Luminescent Spectroscopy of Proteins*, CRC Press, Boca Raton, FL.
38. Eftink, M. R., and Shastry, M. C. R. (1997) *Methods Enzymol. 278*, 258−286.
39. Parker, M. J., Spencer, J., and Clarke, A. R. (1995) *J. Mol. Biol. 253*, 771−785.
40. Goldenberg, D. P. (1988) *Annu. Rev. Biophys. Biophys. Chem. 17*, 481−507.
41. Kuwajima, K. (1989) *Proteins: Struct., Funct., Genet. 6*, 87−103.
42. Nall, B. T. (1994) in *Mechanisms of Protein Folding* (Pain, P. H., Ed.) pp 80−103, Oxford University Press, New York.
43. Jackson, S. E., and Fersht, A. R. (1991) *Biochemistry 30*, 10436−10443.
44. Silow, M., and Oliveberg, B. (1997) *Proc. Natl. Acad. Sci. U.S.A. 94*, 6084−6086.
45. Neri, D., Billeter, M., Wider, G., and Wuthrich, K. (1992) *Science 257*, 1559−1563.
46. Lumb, K. J., and Kim, P. S. (1994) *J. Mol. Biol. 236*, 412−420.
47. Ittah, V., and Haas, E. (1995) *Biochemistry 34*, 4493−4506.

48. Pan, H., Barbar, E., Barany, G., and Woodward, C. (1995) *Biochemistry 34*, 13974−13981.
49. Saab-Rincon, G., Gualfetti, P. J., and Matthews, C. R. (1996) *Biochemistry 35*, 1988−1994.
50. Sosnick, T. R., Mayne, L., Hiller, R., and Englander, S. W. (1994) *Nat. Struct. Biol. 1*, 149−156.
51. Sosnick, T. R., Shtilerman, M. D., Mayne, L., and Englander, S. W. (1997) *Proc. Natl. Acad. Sci. U.S.A. 94*, 8545−8550.
52. Qi, P. X., Sosnick, T. R., and Englander, S. W. (1998) *Nat. Struct. Biol. 5*, 882−884.
53. Baldwin, R. L. (1996) *Folding Des. 1*, R1−R8.
54. Capaldi, A. P., and Radford, S. E. (1998) *Curr. Opin. Struct. Biol. 8*, 86−92.

BI991937J